⌘ *Author's Choice*

THE JOURNAL OF BIOLOGICAL CHEMISTRY VOL. 286, NO. 48, pp. 41801–41811, December 2, 2011

Interactions of Cations with the Cytoplasmic Pores of Inward Rectifier K^+ Channels in the Closed State[S]

Received for publication, July 1, 2011, and in revised form, October 6, 2011 Published, JBC Papers in Press, October 9, 2011, DOI 10.1074/jbc.M111.278531

Atsushi Inanobe[‡§1], Atsushi Nakagawa[¶], and Yoshihisa Kurachi[‡§2]

From the [‡]Department of Pharmacology, Graduate School of Medicine, [§]Center for Advanced Medical Engineering and Informatics, and [¶]Laboratory of Supramolecular Crystallography, Institute for Protein Research, Osaka University, Osaka 565-0871, Japan

Ion channels gate at membrane-embedded domains by changing their conformation along the ion conduction pathway. Inward rectifier K^+ (Kir) channels possess a unique extramembrane cytoplasmic domain that extends this pathway. However, the relevance and contribution of this domain to ion permeation remain unclear. By qualitative x-ray crystallographic analysis, we found that the pore in the cytoplasmic domain of Kir3.2 binds cations in a valency-dependent manner and does not allow the displacement of Mg^{2+} by monovalent cations or spermine. Electrophysiological analyses revealed that the cytoplasmic pore of Kir3.2 selectively binds positively charged molecules and has a higher affinity for Mg^{2+} when it has a low probability of being open. The selective blocking of chemical modification of the side chain of pore-facing residues by Mg^{2+} indicates that the mode of binding of Mg^{2+} is likely to be similar to that observed in the crystal structure. These results indicate that the Kir3.2 crystal structure has a closed conformation with a negative electrostatic field potential at the cytoplasmic pore, the potential of which may be controlled by conformational changes in the cytoplasmic domain to regulate ion diffusion along the pore.

Ion channel pores permit the passage of ions through cell membranes. Their opening and closing (gating) process is controlled by various physiological stimuli, such as the membrane electric field and the extracellular or intracellular ligands. Thus, gating is fundamental to the biological functions of ion channels. Structural analyses of K^+ channels have revealed the presence of strong structural similarities in their membrane-embedded domains, each of which contains an ion conduction pathway at the center of an assembly of four individual subunits (1–4). These analyses have also confirmed the existence of physical constraints on ion conduction at a bundle crossing exerted by inner helices near the cytoplasm and a selectivity filter near the extracellular vestibule (2–5). These constraints are reported to function as an activation gating not only of various K^+ channels (6–8), but also of cyclic nucleotide-gated ion channels (9, 10). Changes in the conformation of structural elements along the ion conduction pathway are therefore crucial in terms of controlling the passage of ions.

Inward rectifier K^+ (Kir)[3] channels possess an extensive cytoplasmic domain (3, 11) that harbors binding sites for various channel regulators (see Fig. 1*A*) (12–14). Association with activators shifts the conformational equilibrium in the domain, leading to restructuring of the transmembrane domain to achieve control of gating (13–15). At the four-fold symmetry axis of the cytoplasmic domain, there is an ion conduction pathway that can be as long as that of the transmembrane domain (3, 11). Crystallographic studies have revealed that although all the Kir channel structures have constraints on ion diffusion through the pore in the transmembrane domain, the cytoplasmic pores are filled with water, and some can accommodate hydrated cations (3, 16–19). Furthermore, intracellular chemical modifiers or cations can enter the central cavity of the transmembrane domain of some Kir channels even when these channels are in their closed states (20, 21). On the other hand, structural analyses of the bacterial homologue Kir channel KirBac3.1 raised the possibility that the cytoplasmic pore might be capable of changing its diameter (18, 22, 23). Clearly, the manner in which the structure of the cytoplasmic pore affects the conduction of ions is still a matter of debate.

Here, we report on our crystallographic and electrophysiological analyses of the interactions of cations with the Kir channel subunit Kir3.2. On the basis of our results, we propose that the Kir3.2 cytoplasmic domain undergoes a conformational change that is potentially linked to the alteration of the strength of the negative electrostatic field potential at its pore. This potential change in conformation of the cytoplasmic domain raises the possibility that the pore makes a critical contribution to the regulation of ion diffusion, although it is located outside the electric field of the membrane.

[S] The on-line version of this article (available at http://www.jbc.org) contains supplemental Figs. S1 and S2.

⌘ *Author's Choice*—Final version full access.

The atomic coordinates and structure factors (codes 3AT8, 3AT9, 3ATA, 3ATB, 3ATD, 3ATE, and 3ATF) have been deposited in the Protein Data Bank, Research Collaboratory for Structural Bioinformatics, Rutgers University, New Brunswick, NJ (http://www.rcsb.org/).

[1] Supported by Grant-in-Aid for Scientific Research (C) 23590301. To whom correspondence may be addressed: Dept. of Pharmacology, Graduate School of Medicine, Osaka University, 2-2 Yamada-Oka, Suita, Osaka 565-0871, Japan. Tel.: 81-6-6879-3512; Fax: 81-6-6879-3519; E-mail: inanobe@pharma2.med.osaka-u.ac.jp.

[2] Supported by Grant-in-Aid for Scientific Research on Innovative Areas 22136002 from the Ministry of Education, Culture, Sports, Science and Technology of Japan. To whom correspondence may be addressed: Dept. of Pharmacology, Graduate School of Medicine, Osaka University, 2-2 Yamada-Oka, Suita, Osaka 565-0871, Japan. Tel.: 81-6-6879-3512; Fax: 81-6-6879-3519; E-mail: ykurachi@pharma2.med.osaka-u.ac.jp.

[3] The abbreviations used are: Kir, inward rectifier K^+; PIP_2, phosphatidylinositol 4,5-bisphosphate; MTS, methanethiosulfonate; MTSES, (2-sulfonatoethyl) methanethiosulfonate; MTSET, [2-(trimethylammonium)ethyl] methanethiosulfonate.

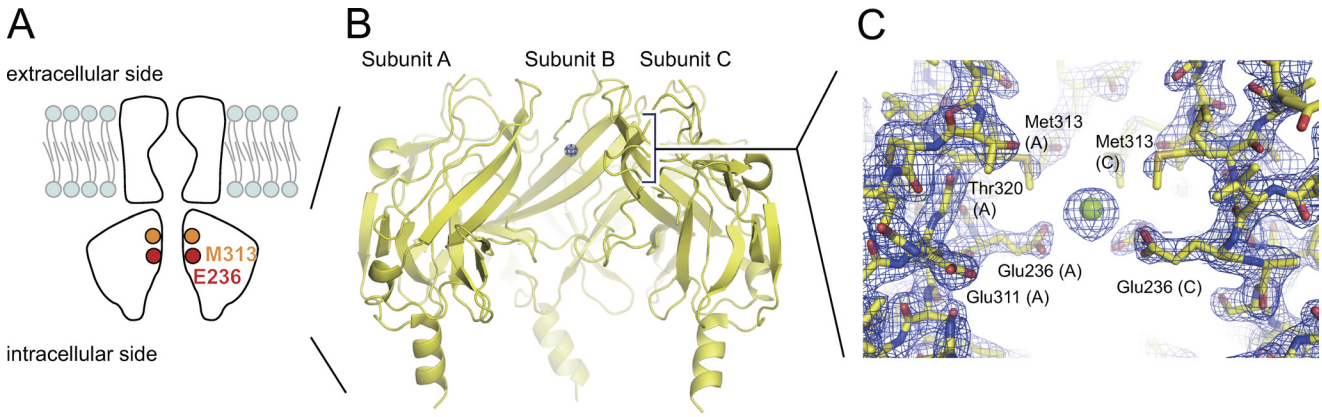

FIGURE 1. **The cytoplasmic pore of Kir3.2.** *A*, domain topology of Kir channels. The Kir channel consists of transmembrane and cytoplasmic domains. The ion conduction pathway is located at the center of a tetrameric assembly. The residues that are involved in interactions between the cytoplasmic domains and cations are indicated. *B*, distribution of the electron density peaks in Kir3.2. A ribbon representation of the cytoplasmic domain of Kir3.2 is presented together with the $F_o - F_c$ ion omit map contoured at 5.0 σ. The front subunit is omitted for clarity. *C*, an enlarged side view of the region around the strong electron density peak. The model is shown as sticks with the composite $2F_o - F_c$ map contoured at 1.5 σ. The Mg^{2+} ion is shown as a *green sphere*.

EXPERIMENTAL PROCEDURES

X-ray Diffraction Measurements and Structural Analyses—The cytoplasmic domain of mouse Kir3.2 is a direct concatemer of its N and C termini. The protein was purified and crystallized in the absence of Na^+, as reported previously (24, 25). After the growth of the crystals was stopped, a solution containing the test cation (2 μl) was mixed with the crystallization solution (2 μl), and then half the mixture was removed. These steps were repeated more than 15 times until the original Mg^{2+} concentration was reduced to less than 10 μM. The replacement solutions contained 10 mM Tris-HCl, pH 8.0, 10% (w/v) sucrose, 5 mM 2-mercaptoethanol, 150 mM KCl, 10% (v/v) ethanol, and 25% (v/v) glycerol; to this we added 10 mM $BaCl_2$, 10 mM $BaCl_2$ plus 10 mM $MgCl_2$, 10 mM $BaCl_2$ plus 10 mM spermine, 10 mM $GdCl_3$, 10 mM $GdCl_3$ plus 10 mM $MgCl_2$, or 10 mM praseodymium acetate ($Pr(OAc)_3$). In the case of cesium, we added 200 mM CsCl instead of KCl and $MgCl_2$. When the solution had been replaced, the crystals were mounted on nylon pins and immersed directly in liquefied nitrogen. All procedures were carried out at 4 °C.

The main data were collected at the BL44XU beam line at the SPring-8 synchrotron radiation facility (Hyogo Prefecture, Japan), whereas preliminary data were collected at the 13B1 beam line at the National Synchrotron Radiation Research Center in Taiwan. The data were indexed and scaled by using the HKL2000 suite (26). The initial phase was determined by molecular replacement using the coordinates of the cytoplasmic domain of Kir3.2 (Protein Data Bank (PDB) code: 3AGW) (25). Model refinement was carried out with programs in the CCP4i suite (27) and the graphics program Coot (28). The location of the replacement cations was defined by using their anomalous Fourier maps. The $F_o - F_c$ ion omit maps were calculated from the refined Kir3.2 structures without cations. The statistics of the crystallographic analyses are presented in Table 1. The illustrations of the structures were prepared by using PyMOL (53).

Electrophysiological Analyses—The cDNA of mouse Kir3.2d (29) was subcloned into the expression vector pcDNA3 (Invitrogen) and transfected with porcine m_2-muscarinic receptor into HEK293T cells by using Lipofectamine reagent (Invitrogen). Point mutations were introduced by using a QuikChange site-directed mutagenesis kit (Stratagene; La Jolla, CA), and their presence was confirmed by direct DNA sequencing. In the cysteine-free mutant (C1234), cysteine residues at positions 65, 190, 221, and 321 were replaced by valine, serine, threonine, and valine residues, respectively (30). Inward Kir currents were recorded at a holding potential of −100 mV in excised inside-out patches by using a patch clamp amplifier (Axopatch 200A, Axon Instruments; Grand Terrace, CA). The current was subjected to low pass filtering at 1 kHz and digitized at 10 kHz. Glass pipettes had resistances of 2.5–3.5 megaohms when filled with the pipette solution. The pipette solution contained 135 mM KCl, 1 mM $CaCl_2$, 1.6 mM $MgCl_2$, 5 mM HEPES, and 5 μM acetylcholine. The bath solution consisted of 135 mM KCl, 5 mM EGTA, 2 mM $MgCl_2$, and 5 mM HEPES (pH 7.35 adjusted by KOH). ATP was added to the bath solution to produce phosphatidylinositol 4,5-bisphosphate (PIP_2) at the inner leaflet of the patch membrane. *N*,*N*,*N*-Trimethylethanaminium methanesulfonothioate (MTSET) and 2-sulfonatoethyl methanesulfonothioate (MTSES) (Anatrace Inc.; Maumee, OH) were dissolved in water at 0.1 M and stored at −20 °C until use. Solutions containing 2 mM K_2ATP were freshly prepared each day. The pH of each of the solutions was adjusted to 7.35 with KOH before the experiments. Because the perfusion of NaCl did not shift the zero current level in the presence of 10 μM $CdCl_2$ (30), NaCl was added to the bath solution without compensating for changes in osmolarity and ionic strength. All experiments were performed at ambient temperature (23–25 °C). The data are expressed as mean values ± S.E. Statistical analyses were performed by using Student's *t* test.

RESULTS

In the crystal structure of the cytoplasmic domain of Kir3.2 prepared in the absence of Na^+ (PDB ID 3AGW) (25), we found a strong positive peak in the electron density map in the cytoplasmic pore that could not be accounted for by protein (Fig. 1*B*). The electron density peak is caged by the side chains of Glu-236 and Met-313 that project into the cytoplasmic pore

TABLE 1
Summary of x-ray diffraction data for the cytoplasmic domain of Kir3.2 soaked in solutions containing various cations

Cations	10 mM Ba^{2+}	10 mM Ba^{2+} plus 10 mM Mg^{2+}	10 mM Ba^{2+} plus 10 mM spermine	10 mM Gd^{3+}	10 mM Gd^{3+} plus 10 mM Mg^{2+}	10 mM Pr^{3+}	200 mM Cs^{+}
Data collection statistics							
Space group	I422	I422	I422	I422	I422	I422	I422
Unit cell dimensions	$a = b = 81.833$ Å, $c = 172.463$ Å	$a = b = 81.771$ Å, $c = 172.274$ Å	$a = b = 81.691$ Å, $c = 172.429$ Å	$a = b = 82.373$ Å, $c = 172.810$ Å	$a = b = 82.166$ Å, $c = 172.045$ Å	$a = b = 82.775$ Å, $c = 172.894$ Å	$a = b = 81.732$ Å, $c = 172.125$ Å
No. per a.u.[a]	1	1	1	1	1	1	1
Lambda (Å)	1.6000	1.6000	1.6000	1.46	1.46	1.6	1.5
d min (Å)	3.3	3.3	3.5	3.5	3.0	3.2	2.95
Total observations	108,575	114,340	104,396	104,372	176,319	137.769	338,695
Unique observations	4,084	4,009	3,436	3,241	5,600	4,575	5,985
R_{merge} (%)[b,c]	17.2 (61.4)	18.1 (60.4)	16.3 (56.4)	17.2 (84.6)	17.0 (71.0)	15.0 (60.3)	11.8 (55.8)
Completeness[c]	99.0 (91.1)	99.2 (93.0)	100 (99.7)	99.9 (99.0)	99.4 (95.6)	99.6 (96.0)	99.9 (99.5)
$I / \sigma (I)$[c]	17.7 (2.2)	18.4 (2.5)	23.5 (5.3)	23.0 (3.1)	22.8 (2,6)	21.2 (3.0)	48.4 (5.9)
Redundancy[c]	23.2 (8.1)	24.5 (10.5)	26.1 (17.9)	26.0 (16.2)	28.4 (10.1)	26.3 (10.7)	52.3 (31.1)
Refinement statistics							
Resolution (Å)	30.0-3.3	30.0-3.3	30.0-3.5	30.0-3.5	30.0-3.0	30.0-3.2	30.0-2.95
R_{work} (%)[d]	24.2	23.1	22.1	30.4	25.3	26.7	22.3
R_{free} (%)[e]	28.6	26.9	28.0	34.6	28.3	32.4	28.1
No. of protein atoms	1,574	1,574	1,574	1,574	1,574	1,574	1,552
No. of cations/EtOH/waters	1/0/0	1/0/0	1/0/0	2/0/0	1/0/0	3/0/0	3/2/13
Average B value							
Overall	81.8	74.0	83.5	43.5	74.4	69.0	44.7
Main	81.4	73.9	83.2	41.7	74.0	68.6	44.3
Side chain/ion/EtOH/water	82.1	74.1	83.8	43.8	74.9	69.4	45.2
r.m.s.[f] deviation							
Bonds (Å)	0.010	0.010	0.011	0.012	0.012	0.012	0.012
Angles (°)	1.20	1.19	1.22	1.22	1.35	1.27	1.31
Ramachandran plot[g]	84.0/16.0/0/0	84.0/16.0/0/0	84.6/15.4/0/0	85.1/14.9/0/0	86.9/13.1/0/0	87.4/12.0/0.6/0	84.9/15.1/0/0

[a] Number of protein molecules per asymmetric unit (a.u.).
[b] $R_{merge} = \Sigma^h \Sigma^i (|I^i(h)| - |\langle I(h)\rangle|)/\Sigma^h \Sigma^i I^i(h)$, where $I^i(h)$ is the observed intensity and $\langle I\,(\mathrm{h})\rangle$ is the mean intensity observed from multiple measurements.
[c] Values in parentheses define the resolution range at the highest shell of data.
[d] $R_{work} = \Sigma \||F_o| - |F_c|\|/\Sigma |F_o|$, where F_o and F_c denote observed and calculated structure factors, respectively.
[e] Over 500 reflections were set aside for the calculation of the R_{free} value.
[f] r.m.s., root mean square.
[g] The percentage of amino acids distributed in most favored/allowed/generous/disallowed regions of Ramachandran plot.

from each of the four subunits (Fig. 1*C*). The position of the peak is similar to that of one of the Na^+-binding sites in the Kir3.1/S225E mutant cytoplasmic domain (31), and it is close to that of the binding site for various cations in the full-length chicken Kir2.2 channel (17). These results suggest that the electron density peak corresponds to a cation. The cation is 4.4 Å from the carboxyl oxygen of Glu-236 and 4.5 Å from the sulfur atom of Met-313. Because these distances are much greater than the ionic radius of any cation, the interaction appears to be mediated by water molecules. To identify the cation that is responsible for the electron density peak, we steeped the crystals in crystallization solutions containing various cations, and then we detected the positions of the cations in the crystal structure by means of their anomalous difference signals. No anomalous signal could be observed at this position in the native crystals at wavelengths of 0.815, 0.900, 1.000, 1.500, or 1.600 Å. Therefore, anomalous signals from the crystals are likely to have arisen from cations in the replacement solution and not from trace heavy atom contamination during expression, purification, or crystallization of the protein. The crystal structures of the Kir3.2 cytoplasmic domain with various bound cations are similar to that of the native form; the root mean square deviations of the overall backbone Cα positions are less than 0.32 Å, and those of the Cα positions of Glu-236 and Met-313 in diagonal subunits are less than 0.7 Å. These values are within limits of error of structural models built on the basis of electron density maps of modest resolution. The data collection and refinement statistics are summarized in Table 1.

Interactions between Divalent and Trivalent Cations and the Cytoplasmic Pore—Ba^{2+} can block the outward flow of K^+ from the intracellular side, as does Mg^{2+} (20, 32). When crystals were steeped in a Mg^{2+}-free 10 mM solution of Ba^{2+}, a peak for the Ba^{2+}-derived anomalous difference signal and a positive peak in the $F_o - F_c$ ion omit map were detected in the cytoplasmic pore (Fig. 2*A*). The position of Ba^{2+} is equivalent to that of the electron density peak in the native crystal form, strongly suggesting that the electron density peak in the cytoplasmic pore in the native form corresponds to a cation. The calculated density of the peak of the Ba^{2+}-derived anomalous signal was 6.62×10^{-2} electrons/Å^3 (e/Å^3), but this value decreased to 3.83×10^{-2} e/Å^3 in the presence of an equimolar concentration of Mg^{2+} (Fig. 2*B*). In addition to decreasing the strength of the anomalous signal peak for Ba^{2+}, Mg^{2+} also reduced the area and the peak height in the $F_o - F_c$ ion omit map. Because Ba^{2+} has a greater x-ray scattering power than does Mg^{2+}, binding of Ba^{2+} to the cytoplasmic pore appears to compete with binding of Mg^{2+}. The distribution of Ba^{2+} in the cytoplasmic pore extends to the area surrounded by the carboxyl groups of the Glu-236 moieties in each of the four subunits. Two Ba^{2+} ions cannot be present at this site because the distance between them would be about 1 Å, a distance that is too small to accommodate the electrical repulsion between the ions. Therefore, Ba^{2+} appears to position itself over a greater proportion of the cytoplasmic pore than does Mg^{2+}.

Spermine (*N*,*N*′-bis(3-aminopropyl)butane-1,4-diamine) is an endogenous substance that also causes inward rectification by Kir channels (33). We tested the effects of spermine on bind-

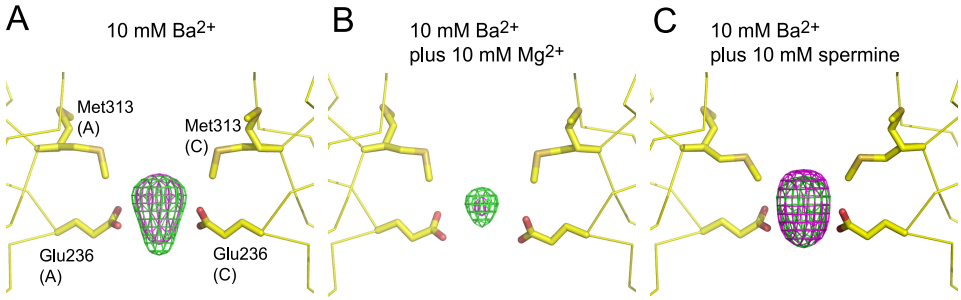

FIGURE 2. **Interactions of Ba^{2+} with the cytoplasmic domain of Kir3.2.** *A*, the crystal of the Kir3.2 cytoplasmic domain was steeped in a Mg^{2+}-free solution that contained 10 mM Ba^{2+}. *B* and *C*, other crystals were soaked in the same solution with the addition of either 10 mM Mg^{2+} (*B*) or 10 mM spermine (*C*). The anomalous signals of Ba^{2+} (*purple mesh* contoured at 4.0 σ) and the $F_o - F_c$ ion omit map (*green mesh* contoured at 5.0 σ) at the cation-binding site are shown with *ribbons* representing two diagonally symmetric subunits and *sticks* representing Glu-236 and Met-313.

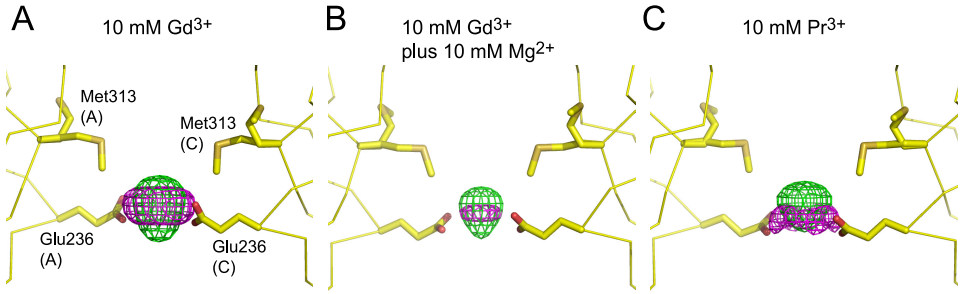

FIGURE 3. **Interaction of trivalent cations with the Kir3.2 cytoplasmic domain.** *A–C*, these anomalous difference maps (*purple*) and $F_o - F_c$ ion omit maps (*green*) were obtained from crystals soaked in solutions containing 10 mM Gd^{3+} (*A*), 10 mM Gd^{3+} and 10 mM Mg^{2+} (*B*), or 10 mM Pr^{3+} (*C*). The anomalous maps are contoured at 7.5 σ for *A* and *B* and at 9.0 σ for *C*. The contour level for the $F_o - F_c$ ion omit maps is 9.0 σ.

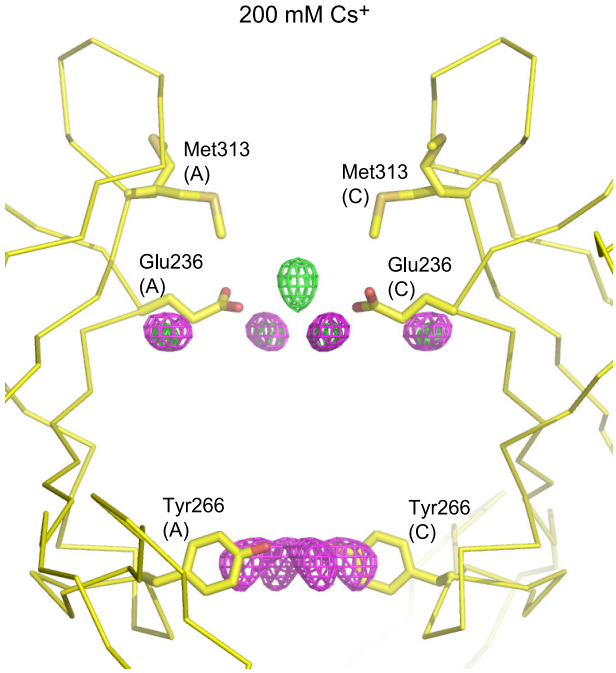

FIGURE 4. **Interaction of the monovalent cation Cs^+ with the cytoplasmic domain of Kir3.2.** The anomalous difference map (*purple mesh* contoured at 6.0 σ) and the $F_o - F_c$ ion omit map (*green mesh* contoured at 5.0 σ) were obtained from a crystal soaked in a solution free of Mg^{2+} and K^+ that contained 200 mM Cs^+. The two diagonally symmetric subunits (*A* and *C*) of Glu-236, Tyr-266, and Met-313 are shown as *ribbons*, and the side chains are shown as *sticks*. See also supplemental Fig. S1.

ing of Ba^{2+} to the cytoplasmic pore (Fig. 2*C*). In the presence of spermine, the density of the Ba^{2+}-derived anomalous signal was 6.44 × 10^{-2} e/Å^3, a value that is comparable with that found in the absence of competitors. This shows that spermine does not compete with Ba^{2+}. Although spermine has a valency of +4 at physiological pH values, each charge has a monovalent character, suggesting that binding of cations to the cytoplasmic domain may depend on the valency of the positively charged moiety.

Next, we examined the binding of the trivalent cations Gd^{3+} and Pr^{3+} to the cytoplasmic pore. Both cations were found near the positive electron density peak seen in the native form (Fig. 3, *A* and *C*). However, their position was shifted by 0.9 Å toward the cytoplasm, although it remained within the extended area that can be occupied by Ba^{2+} (Fig. 2*A*). The inclusion of Mg^{2+} reduced the heights of both the $F_o - F_c$ positive and the Gd^{3+}-derived anomalous signal peaks, indicating the presence of competitive binding (Fig. 3*B*). These results suggest that multivalent cations interact with a site in the cytoplasmic pore of Kir3.2 and that their physical properties lead to minute differences in their localization within the pore.

Interaction of Monovalent Cations with the Cytoplasmic Pore—We tested whether monovalent cations associate with the cation-binding site in the Kir3.2 cytoplasmic pore. When crystals were soaked in a 200 mM solution of Cs^+ that was free of Mg^{2+} and K^+, two obvious anomalous signal peaks were observed in the cytoplasmic pore (Fig. 4). The first Cs^+ was located near the multivalent cation-binding site described above; at this site, Cs^+ is docked in an anionic environment that is surrounded by the carboxyl oxygen atoms of Glu-236 and Glu-311, the hydroxy oxygen atom of Ser-238, and the carboxyl oxygen atom of Glu-236 in the adjacent subunit (supplemental Fig. S1*C*). The second Cs^+ was located at the cytoplasmic entrance of the pore and was surrounded by Tyr-266 (supplemental Fig. S1*D*). Tyr-266 interacted extensively with Cs^+, and the distance between

the Cs^+ ion and the phenyl ring was 3.8 Å. The distance between the two Cs^+ ions was 3.9 Å. In contrast to the obvious anomalous signal of Cs^+, the temperature factors of the first and second Cs^+ ions were 143.3 and 159.7, respectively, and the average temperature factors of atoms involved in the interaction with the first and second Cs^+ ions were 39.5 and 44.5, respectively, suggesting low occupancies. Because Cs^+ has a lower hydration energy (−71 kcal mol^{-1}) and a larger ionic radius (1.69 Å) than does K^+ (−105 kcal mol^{-1} and 1.33 Å, respectively), we tested the distribution of Rb^+, which can permeate through Kir channels (supplemental Fig. S1*A*). The occupancy of Rb^+ was also low, but its anomalous signal was detectable at the first Cs^+-binding site. Therefore, the position of monovalent cations in the cytoplasmic pore is dependent on the valency of the cation but independent of its physical characteristics.

Although a positive electron density peak in the $F_o - F_c$ ion omit map was detected at the cation-binding site, anomalous signals for only Cs^+ (Fig. 4) or Rb^+ (supplemental Fig. S1*A*) were observed at this site. As a consequence of the serial replacement of solutions, the concentrations of Mg^{2+} and K^+ were expected to be below 10 μM. The monovalent cation (Cs^+ or Rb^+; 200 mM) was therefore the dominant cation in the corresponding crystal. Because Mg^{2+} competes with multivalent cations in binding to the cation-binding site in the presence of 150 mM K^+ (Figs. 2 and 3), it is likely that the affinity of monovalent cations for the site is less than that of Mg^{2+} and that the strong electron density peak at the cytoplasmic pore in the native Kir3.2 crystal can be considered to arise from Mg^{2+} (Fig. 1). This is consistent with the observation that the tetraamine spermine has no effect on binding of Ba^{2+} to the cation-binding site (Fig. 2*C*), thereby strongly supporting the idea that binding is dependent on the valency of the charged moiety of the cation.

Chemical Modification of the Side Chain of Amino Acids Facing the Cytoplasmic Pore—Next we tried to determine how the mode of Mg^{2+} binding couples with functional states of the G protein-gated Kir channels. We generated a cysteine-free mutant (C1234) in which the four cysteine residues that are potentially exposed to the cytoplasm were replaced (30). These residues were as follows: Cys-65 in the N-terminal portion of the cytoplasmic domain, Cys-190 in the second transmembrane helix, and Cys-221 and Cys-321 in the βC and βI strands, respectively, of the C-terminal portion of the cytoplasmic domain. We then introduced a cysteine at either Glu-236 or Met-313 (designated E236C/C1234 and M313C/C1234, respectively) to test the accessibility of this position to solvent from the intracellular side by means of covalent modification with two differently charged thiol reagents: positively charged MTSET or negatively charged MTSES (Fig. 5*A*).

In the presence of Na^+ (100 mM), which leads to activation of the channel, sulfhydryl modifiers applied to the internal surface of excised inside-out patches rapidly inhibited Kir3.2 wild-type (WT) activity, as shown in Fig. 5*A*, where the Kir3.2 channel activity was irreversibly blocked by MTSET (Fig. 5*A*, *panel a*) or by MTSES (Fig. 5*A*, *panel b*) at a concentration of 0.5 mM (30, 34, 35). The similar time courses of inhibition by these MTS reagents implied that the modification was apparently insensitive to the charge on the compound. The C1234 mutant was functional and apparently insensitive to internal MTSET and MTSES (0.5 mM) (Fig. 5*B*). However, the perfusion of these thiol modifiers slightly, but reversibly, reduced the activity of the C1234 mutant, suggesting that they caused nonspecific and noncovalent modifications. Introduction of an additional cysteine residue rendered the resulting E236C/C1234 and M313C/C1234 mutants sensitive to MTSET (Fig. 5, *C*, *panels a* and *b*). However, negatively charged MTSES (0.5 mM) had almost no effects on the activity of the E236C/C1234 mutant (Fig. 5*C*, *panel a*) and slowly decreased the activity of the M313C/C1234 mutant (Fig. 5*C*, *panel b*). Although it is not clear why MTSES can access the side chain at position 313, which is located deeper from the cytoplasm than that at position 236, this result suggested that the cytoplasmic pore could be a selective barrier for charged molecules, through preferential binding of positively charged molecules to negatively charged ones. The decrease in current amplitude resulting from modification by the MTS reagents is presumably a direct result of physical constraints on ionic flow in the cytoplasmic pore and/or an indirect result of perturbational conformational changes that lead to channel opening. In these two channels, inhibition by MTSET occurred with a monoexponential time course. MTSET attenuated E236C/C1234 mutant currents (time constant: 33 ± 4 s, $n = 10$) and M313C/C1234 mutant channel currents (36 ± 2 s, $n = 9$) with comparable time constants.

Because the bath solution contained 2 mM Mg^{2+}, we tried to chelate Mg^{2+} in the solution by adding EDTA (10 mM) to reduce the effect of Mg^{2+} on the thiol modification (Fig. 6, *A*, *panel a* and *B*, *panel a*). Chelation of Mg^{2+} enhanced the activity of E236C/C1234 and M313C/C1234 mutants, and a high concentration of Mg^{2+} (10 mM) tended to attenuate the activity of both mutants (Fig. 6, *A*, *panel b* and *B*, *panel b*). Because not only these mutants, but also Kir3.2 WT and other mutants, showed a similar sensitivity to Mg^{2+} in the presence and the absence of channel activator (Figs. 6 and 7), Mg^{2+} appears to modulate Kir3.2 activity at millimolar concentrations. At a low concentration of Mg^{2+} (0.6 μM) (Fig. 6, *A*, *panel a* and *B*, *panel a*), MTSET blocked the currents of the E236C/C1234 mutant (35 ± 3 s, $n = 4$) and the M313C/C1234 mutant (33 ± 1 s, $n = 3$). Because these time courses of channel blocking by MTSET were similar to those without the Mg^2 chelation, it appeared that the functional Kir3.2 channel may possess a reduced sensitivity to Mg^{2+} at the cytoplasmic pore.

Next, we tested the effect of Mg^{2+} at 10 mM on the MTSET modification by supplementing the bath solution with 8 mM Mg^{2+} (Fig. 6, *A*, *panel b* and *B*, *panel b*). Although the modification rate for the E236C/C1234 mutant (35 ± 2 s, $n = 4$) was similar to that in a low concentration of Mg^{2+}, the rate for the M313C/C1234 mutant (57 ± 7 s, $n = 3$) was slower in the presence of Mg^{2+} than that of the control ($p = 0.04$). This suggested that the chemical modification of the side chain from the intracellular side at position 313, but not at 236, could be prevented by Mg^{2+} at 10 mM.

Mg^{2+} Interacts with Kir3.2 Cytoplasmic Domain in a Closed State—Because homomeric Kir3.2 produces a spiky channel with short open times (<0.5 ms) (13), it is unclear whether

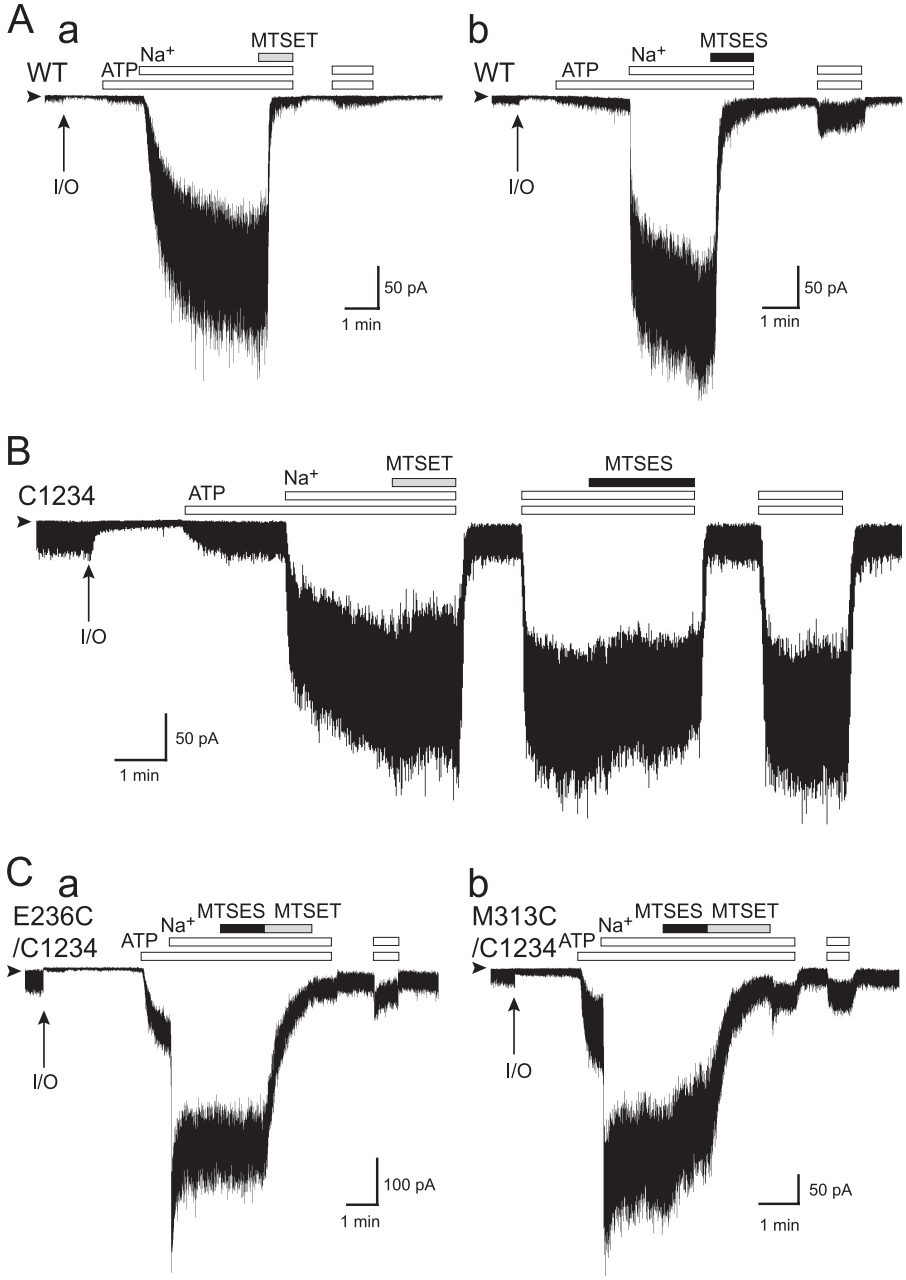

FIGURE 5. **Internal accessibility of the sulfhydryl modifiers to residues facing the cytoplasmic pore of Kir3.2 channels in the presence of channel activator.** Inside-out membrane patches (*I/O*) were obtained from HEK293T cells expressing either Kir3.2 WT or mutant channels. Experiments were conducted in symmetric 135 mM K^+ solutions with a holding potential of −100 mV. The protocol of perfusion of substances to the intracellular side of the patch membrane is indicated by *bars* above the current traces. *A*, the WT channel activated by ATP and Na^+ was irreversibly blocked by positively charged MTSET (*panel a*) or negatively charged MTSES (*panel b*) at concentrations of 0.5 mM. *B*, the C1234 mutant with substitution of cysteines at positions 65, 190, 221, and 321 by valine, serine, threonine, and valine, respectively, was apparently insensitive to MTSET and MTSES in the presence of Na^+. *C*, the introduction of cysteine into the C1234 mutants at either Glu-236 (E236C/C1234) or Met-313 (M313C/C1234) restored sensitivity to MTSET. However, the E236C/C1234 mutant was almost insensitive to MTSES (0.5 mM), and the M313C/C1234 mutant was less sensitive to it. In the patch current records, the *arrowheads* indicate the zero current levels, and *arrows* (*I/O*) indicate when the patch was excised.

Mg^{2+} protection of the side chain at position 313 by MTSET modification is dependent on the existence of an open or closed state. To address this point, we tried to assess the effect of the modification on the closed state by comparing the current amplitudes elicited by Na^+ before and after the application of MTSET. The replacement of four cysteine residues gave a mutant whose current amplitude ran down with a variable rate and to a variable extent. However, the mutant channels in some patches did not exhibit a decline in the current. This made it difficult to assess the state dependence of the modification by using the mutants.

The activation of G-protein-gated Kir channels is triggered by the associations of $G\beta\gamma$ and Na^+, leading to an increase in affinity to PIP_2 (36–38). The WT channel can, therefore, be slightly activated by the perfusion of PIP_2 or by ATP, which generates PIP_2 at the inner leaflet of the excised patch membrane. The current amplitude would be less than 0.1% of that produced by 100 mM Na^+ (Fig. 5*A*) (25). The activation of the

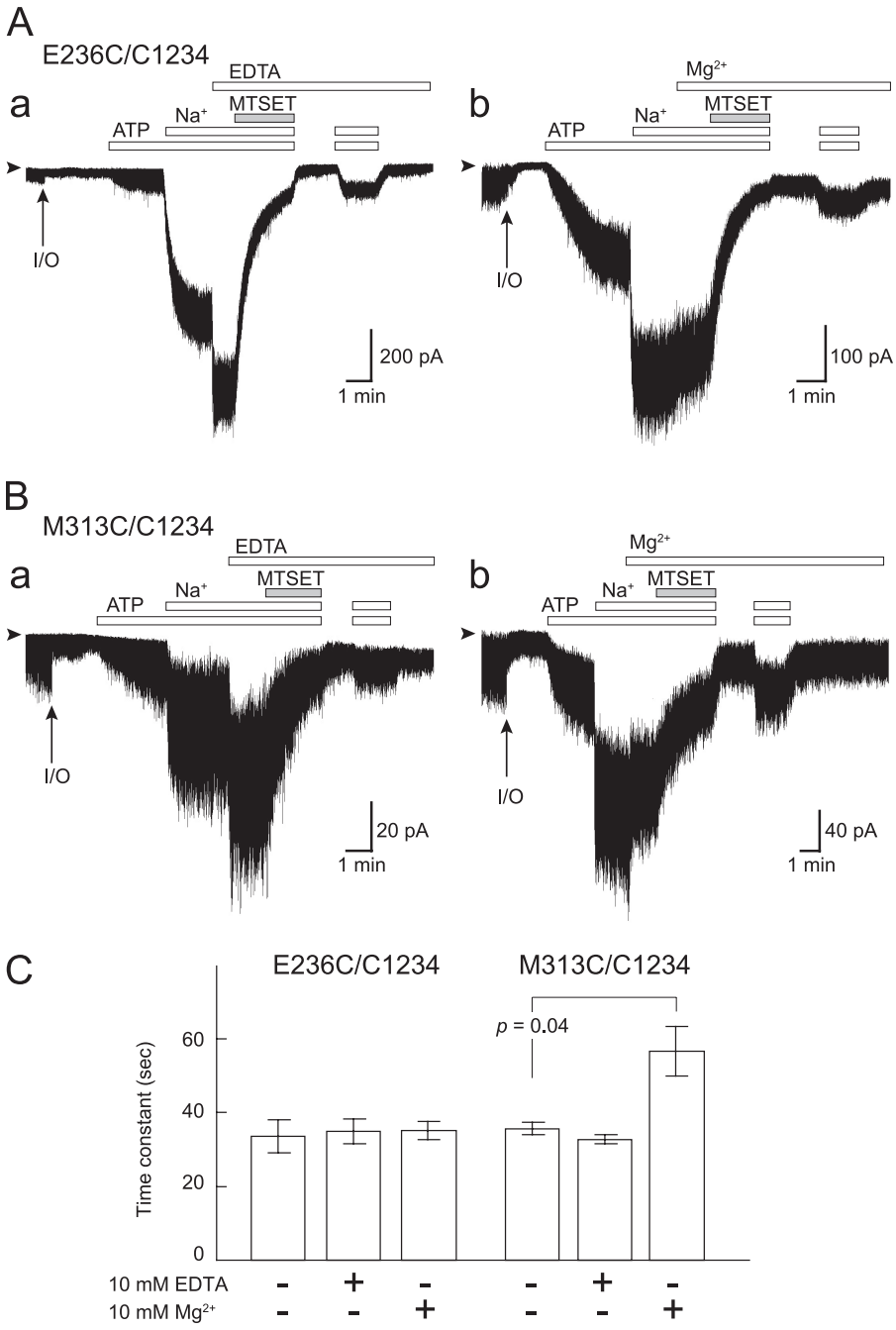

FIGURE 6. **The effect of Mg^{2+} on MTSET modification of Kir3.2 channel mutants in the presence of channel activator.** *A* and *B*, to examine the effects of Mg^{2+} on MTSET modification (0.5 mM) for E236C/C1234 (*A*, *panel a*) and M313C/C1234 mutants (*B*, *panel a*), EDTA (10 mM) was perfused to reduce the Mg^{2+} concentration to about 0.6 μM. By adding Mg^{2+} to the bath solution, the effect of high concentration of Mg^{2+} (10 mM) was also tested for E236C/C1234 (*A*, *panel b*) and M313C/C1234 mutants (*B*, *panel b*). *I/O*, inside-out membrane patches. *C*, quantitative comparison of current modification by MTSET. Averaged current modification time constants for MTSET with two mutants in two different concentrations of Mg^{2+} are shown. The time constant (τ in seconds) was calculated by the following equation: $I(t) = I_{max} \times (1 - \exp(-t/\tau)) + A$, where $I(t)$ and I_{max} are the respective relative and maximal current amplitudes (pA), t is the time (in seconds), and A is a constant value (pA). *Error bars* are S.E.

channels is thought to be based on an increase in the probability of the channel being open, and it has no effect on single-channel conductance (39, 40). This shows that although the introduction of mutations at cysteine and at the pore residues resulted in an increase in the basal current amplitudes (Figs. 5–7), we might expect that when a WT or mutant channel conducts K^+ ions, the shape of the ion conduction pathway is functionally equivalent in both the basal and the activated states and that the major difference between these states is in the population of the channel or, in other words, whether it is open or closed. The rates for modification recorded in the absence and the presence of Na^+ should therefore reflect a measure of the exposure of cysteine in the closed and open channel conformations, respectively. We therefore examined the effects of MTSET (0.5 mM) on the basal current of mutants after we had confirmed that we had achieved an inside-out patch configuration by activating the channels with 100 mM Na^+ (Fig. 7 and supplemental Fig. S2).

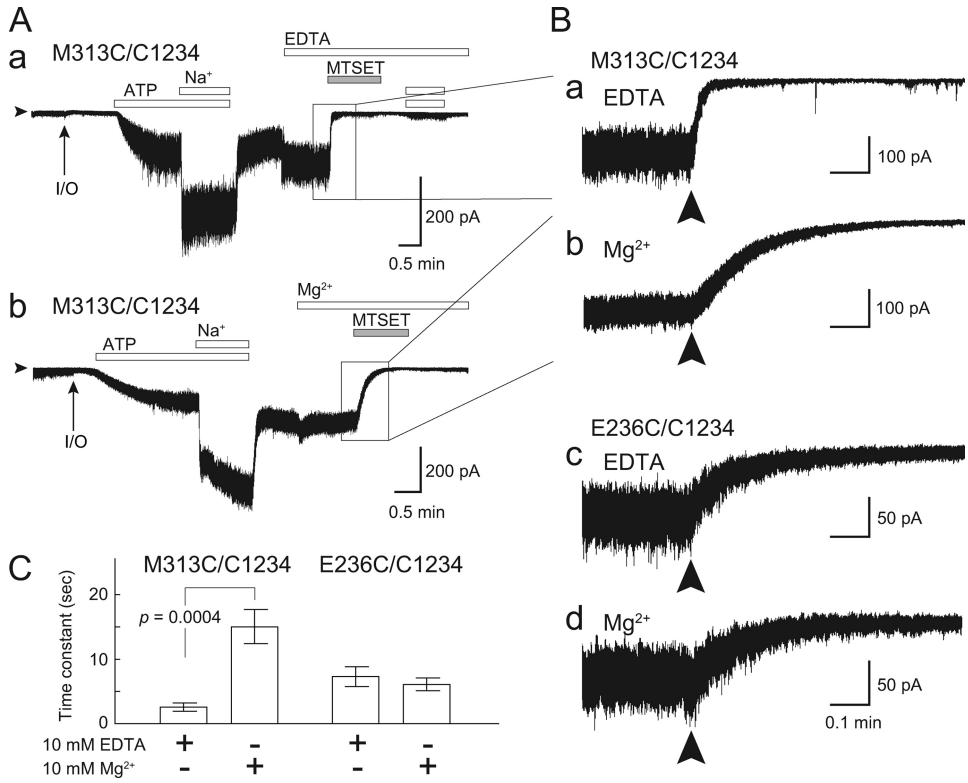

FIGURE 7. **Accessibility of MTSET along the cytoplasmic pore of Kir3.2 mutants in the absence of channel activator.** *A*, following activation of the M313C/C1234 mutant channel by 100 mM Na^+, MTSET (0.5 mM) was perfused at low (0.6 μM; *panel a*) or high concentrations of Mg^{2+} (10 mM; *panel b*). *I/O*, inside-out membrane patches. *B*, the current trace for the M313C/C1234 mutant during the application of MTSET in *A*, *panel a* (highlighted by a *rectangle*) is enlarged in *B*, *panel a*, and that in *A*, *panel b* is correspondingly enlarged in *B*, *panel b*. Similar experiments were performed with the E236C/C1234 mutant (supplemental Fig. S2), and the effects of MTSET on the basal currents at low and high concentrations of Mg^{2+} are enlarged in *B*, *panels c* and *d*, respectively. The time points when the patch was exposed to the solution containing MTSET are indicated by *arrowheads* in *B*. *C*, the time constants for apparent MTSET modification. Data shown represent means ± S.E. See also supplemental Fig. S2.

MTSET attenuated the basal currents in the E236C/C1234 and M313C/C1234 mutant channels faster in the absence of Na^+ than in its presence (Figs. 6 and 7 and supplemental Fig. S2). The rapid modification in the absence of Na^+ suggests that internal MTSET has easy access to the side chains at positions 236 and 313 when Kir3.2 is in its closed state. In the presence of EDTA (10 mM), internal MTSET rapidly attenuated the basal current in the M313C/C1234 mutant (2.6 ± 0.6 s, $n = 10$), whereas in the presence of Mg^{2+} (10 mM), the mutant showed a significant delay in the basal current on MTSET modification (15 ± 3 s, $n = 11$; $p = 0.0004$) (Fig. 7). This obviously showed that Mg^{2+} inhibits the modification of the side chain at position 313, probably through interference with access by MTSET. Furthermore, in this basal condition, Mg^{2+} slowed MTSET modification at position 313 by a factor of six (Fig. 7), whereas in the presence of Na^+, Mg^{2+} slowed the modification by a factor of 1.6 (Fig. 6). This indicates that the channel has a higher sensitivity to Mg^{2+} at a low probability of being open and implies that although the affinity between Mg^{2+} and the open conformation remains to be clarified, Kir3.2 in a closed state has a high affinity for Mg^{2+}. On the other hand, the time constant of the MTSET modification for the E236C/C1234 mutant channel was unaffected by the presence (6.1 ± 1.0 s, $n = 7$) or absence (7.3 ± 1.5 s, $n = 7$) of Mg^{2+}. The selective blocking by Mg^{2+} of this modification suggests that the channel in its closed state tends to bind Mg^{2+} at a site between the side chains of Glu-236 and Met-313 and that the mode of binding is likely to be similar to that observed in the crystal structure of the Kir3.2 cytoplasmic domain (Fig. 1). Therefore, the crystal structure of the Kir3.2 cytoplasmic domain appears to be linked to the closed state of the functional channel.

DISCUSSION

Crystal Structures of the Kir3.2 Cytoplasmic Pore Represent the Closed Conformation—Conformational changes along the ion conduction pathways in the membrane-embedded domains of ion channels are closely coupled to the action of gating of ion diffusion. In this study, we focused on the ion conduction pathway in the cytoplasmic domain of the Kir channel, which is located outside the electric field of the membrane. In the crystals of the cytoplasmic domain of Kir3.2, the cation-binding site at the pore binds Mg^{2+}, which can be replaced by multivalent cations (Figs. 2 and 3), but not by monovalent cations (Fig. 4 and supplemental Fig. S1). Functional analysis showed the existence of selective binding of cations at the cytoplasmic pore (Fig. 6), acceleration of the modification on lowering the probability of the pore being open (Figs. 6 and 7), and selective blocking by Mg^{2+} of MTSET modification of a side chain at position 313 (Fig. 7). We therefore propose that the water-filled pore in the Kir3.2 cytoplasmic domain adopts a closed conformation and is nonconductive when it binds Mg^{2+} (Fig. 8). This idea is supported by the observations that the crystal structures of the isolated cytoplasmic domain of Kir channels (11, 24, 31, 41) are comparable with those in full-

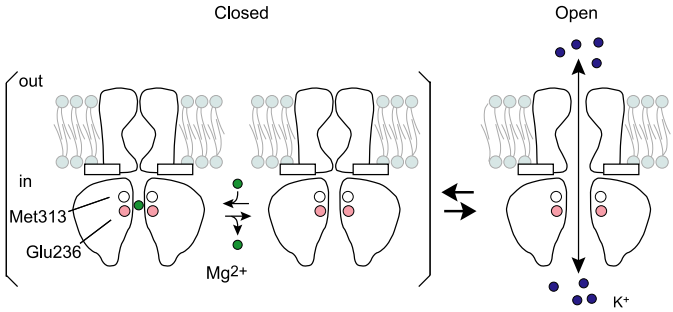

FIGURE 8. **Schematic representation of conformational changes coupled to gating.** Although the membrane-embedded domain of the Kir channel probably gates at the bundle crossing formed by the inner helices near the cytoplasm and the selectivity filter near the extracellular vestibule, the cytoplasmic domain of the channel changes its conformation to alter the electrostatic field potential at the cytoplasmic pore. The pore, in its closed state, tends to bind Mg^{2+}, which prevents diffusion of K^+ ions. When the channel is open, expansion of the cytoplasmic pore lowers the potential and liberates bound Mg^{2+} to permit movement of K^+.

length channels with physical constraints for ion conduction at their transmembrane domains (3, 16–18).

There is a clear discrepancy between the affinity toward Mg^{2+} of the cytoplasmic pore in the crystals (Figs. 2–4) and that in the functional channel (Figs. 6 and 7). There are at least two possible explanations for this discrepancy. The first is that the functional channel has a low probability of being in the conformation observed in the crystal structures. It has recently been reported that the crystal structure of Kir2.2 in a complex with PIP_2 has a narrow opening at the helix bundle crossing of the transmembrane domain (19). Because the crystal structure is known to be a stable conformation of a protein, it is reasonable to postulate that the gating of Kir channels is supported by multiple conformational states. The second possibility is that the electrostatic field potential at the cytoplasmic pore in the crystal structures has been overestimated. In comparison with the condition for recording of channel activity, the domain in the crystals was outside the influence of the transmembrane domain and the cell membranes. Furthermore, although the crystal packing did not perturb the displacement of bound Mg^{2+} by multivalent cations (Figs. 2 and 3), the crystal contacts obviously constrained the possible conformational changes within the domain. The present study, therefore, has a clear limitation in terms of addressing these possibilities. Nevertheless, neither of the cases excludes the possibility that the cytoplasmic pore is electrostatically associated with Mg^{2+} when it is in a closed state.

Molecular Basis of Cation Recognition by the Cytoplasmic Pore—Mutational analysis showed that the cytoplasmic pore of Kir3.2 is much more sensitive to positively charged MTSET than to negatively charged MTSES and that the side chains of both Glu-236 and Met-313 are not principally responsible for this selectivity (Fig. 5). This observation is consistent with the report that according to calculations, many positively charged and noncharged residues in the cytoplasmic domain of mammalian Kir channels might contribute to the formation of a favorable environment for stabilizing cations at the pore (42).

Because each Kir3.2 mutant can be assumed to have a unique channel property (Figs. 5 and 6), it is difficult to compare the rates of MTS modification between mutants. However, the existence of comparable time constants for E236C/C1234 and M313C/C1234 mutants in the presence of Na^+ (Figs. 5 and 6) led us to speculate that MTS modification of the side chain at position 313 is accelerated by lowering the Mg^{2+} concentration (Fig. 7). The glutamate at position 236 is retained in the M313C/C1234 mutant, but not in E236C/C1234 mutant. Thus, the carboxyl group of Glu-236 appears to be involved in the binding of Mg^{2+} by localizing Mg^{2+} at the cation-binding site and/or augmenting the negative electrostatic field potential at the cation-binding site. This agrees with the effect of the carboxyl group of Glu-236 on the local position of the cation (Figs. 2 and 3). Conversely, to these global and local electrostatic effects, the Met-313 side chain showed a low occupancy in all Kir3.2 crystal structures (Figs. 1–4). Furthermore, although the E236C/C1234 mutant retained a methionine residue at position 313, the mutant was insensitive to Mg^{2+} (Fig. 7 and supplemental Fig. S2). Because the electrostatic force cannot act as a basis for specific binding without any geometrical constraints, the structural flexibility around the cation-binding site (*e.g.* the Met-313 side chain) may influence the positioning of the water molecules that hydrate Mg^{2+} bound at the site. By the present study, the role of this residue in the binding of cations remained to be clarified.

Glu-236 and Met-313 are well conserved within the strong inward rectifiers. Glutamate residues equivalent to Glu-236 in other strong inward rectifiers are known to play a role in the attraction of positive charges and to affect the conduction of K^+ and pore blocking by Mg^{2+} and polyamines; they therefore make an essential contribution to the open channel characteristics of ion conduction (43–46). Both the negative electrostatic field potential and the localized charges on side chains, which play key roles in binding of cations in the cytoplasmic pore, contribute to the broad specificity toward cationic molecules or ions when the channel is in its open state.

Mg^{2+} and polyamines are endogenous substances that block the outward flow of K^+ ions (33, 47, 48). Because polyamines cause a stronger inward rectification of Kir channels than does Mg^{2+}, the magnitude of the outward current should be regulated by competitive binding of these substances (49, 50). Mg^{2+} bound at the cation-binding site prevented not only the binding of monovalent cations (Fig. 4), but also the binding of spermine (Fig. 2). Therefore, preferential binding of Mg^{2+} to the cytoplasmic pore in the closed state may be involved in the control of the outward, physiologically relevant, flow of K^+.

Potential Conformational Changes in the Cytoplasmic Domain of Kir Channels—The evidence that multivalent cations replace Mg^{2+} without any disruption of the crystal lattice (Figs. 2 and 3) indicates that no large conformational change is required for access to the cation-binding site by cations from outside the pore. This agrees with the observation that in the absence of Mg^{2+}, chemical compounds or cations can pass through the cytoplasmic pore, thereby gaining access to the central cavity of the closed channel (20, 21). These results suggest that the cytoplasmic pore is capable of allowing passage by cations even in its closed state, which obviously contradicts the idea that the crystal structures of the Kir3.2 cytoplasmic domain are associated with their nonconductive closed state, as discussed above. However, the valency-dependent interaction

is the mechanism responsible for the association between cations and the pore. Because the electrostatic field potential that governs the binding is sensitive to distance, the change in strength of the potential can be controlled by a change in the inner diameter of the cytoplasmic pore (Fig. 8). KirBac3.1 appears to be capable of changing the diameter of its cytoplasmic pore (18, 22, 23). Calculations made by using the Poisson-Boltzmann equation suggest that the electrostatic field potential of the cytoplasmic pore in homology models of eukaryotic Kir channels is too negative to permit the conduction of even K^+ ions (42). Therefore, an expansion of the inner diameter of the pore is probably the most relevant occurrence that leads to liberation of bound Mg^{2+} to permit movement of K^+ when the channel is open (Fig. 8).

At present, the open conformations of both the transmembrane and the cytoplasmic domains of Kir channels are not known at the atomic level. It has been proposed that the G loop following the βH strand in which the Met-313 residue is located is a structural element in the control of gating by mammalian Kir channels (16, 41). The G loop and an adjacent CD loop are known to be flexible (11, 15, 24, 41, 51), and the Glu-236 on the CD loop faces the cytoplasmic pore in Kir3.2 (Fig. 1). These two loops are reported to change their accessibility to the solvent (52), and the N terminus next to the CD loop probably changes its conformation during KirBac3.1 gating (18). Furthermore, the ionic bond between the N terminus and the CD loop appears to stabilize the closed conformation of G protein-gated Kir channels (25), and the tethering of these elements is responsible for the high affinity blocking of Kir3.2 by internal Cd^{2+} (30). These local changes in the conformation of each subunit, as well as a rearrangement of the subunit interface (18) and a displacement of the cytoplasmic domain (17, 19), may control the dilation of the cytoplasmic pore.

We have shown that the pore configuration in the crystal structure of the cytoplasmic domain of Kir3.2 corresponds to the closed conformation of the ion channel. The conformational changes in the domain might be expected to regulate the strength of the electrostatic field potential along the cytoplasmic pore. Therefore, not only might the cytoplasmic domain function as a hub for various channel regulators that control the gate in the transmembrane domain, but it might also participate intimately in rectification and permeation, although the domain is located outside the electric field of the membrane.

Acknowledgments—We thank Tomohito Okada, Yukiko Nishida, and Chizuru Tsuzuki for technical assistance. We are grateful to Dr. Ian Findlay (EA 4433, Faculté des Sciences, Université de Tours, France) for scientific comment for this manuscript.

REFERENCES

1. Doyle, D. A., Morais Cabral, J., Pfuetzner, R. A., Kuo, A., Gulbis, J. M., Cohen, S. L., Chait, B. T., and MacKinnon, R. (1998) *Science* **280,** 69–77
2. Jiang, Y., Lee, A., Chen, J., Cadene, M., Chait, B. T., and MacKinnon, R. (2002) *Nature* **417,** 523–526
3. Kuo, A., Gulbis, J. M., Antcliff, J. F., Rahman, T., Lowe, E. D., Zimmer, J., Cuthbertson, J., Ashcroft, F. M., Ezaki, T., and Doyle, D. A. (2003) *Science* **300,** 1922–1926
4. Long, S. B., Campbell, E. B., and Mackinnon, R. (2005) *Science* **309,** 897–903
5. Cuello, L. G., Jogini, V., Cortes, D. M., Pan, A. C., Gagnon, D. G., Dalmas, O., Cordero-Morales, J. F., Chakrapani, S., Roux, B., and Perozo, E. (2010) *Nature* **466,** 272–275
6. Liu, Y., Holmgren, M., Jurman, M. E., and Yellen, G. (1997) *Neuron* **19,** 175–184
7. del Camino, D., and Yellen, G. (2001) *Neuron* **32,** 649–656
8. Bruening-Wright, A., Schumacher, M. A., Adelman, J. P., and Maylie, J. (2002) *J. Neurosci.* **22,** 6499–6506
9. Flynn, G. E., and Zagotta, W. N. (2001) *Neuron* **30,** 689–698
10. Contreras, J. E., Srikumar, D., and Holmgren, M. (2008) *Proc. Natl. Acad. Sci. U.S.A.* **105,** 3310–3314
11. Nishida, M., and MacKinnon, R. (2002) *Cell* **111,** 957–965
12. Bichet, D., Haass, F. A., and Jan, L. Y. (2003) *Nat. Rev. Neurosci.* **4,** 957–967
13. Hibino, H., Inanobe, A., Furutani, K., Murakami, S., Findlay, I., and Kurachi, Y. (2010) *Physiol. Rev.* **90,** 291–366
14. Lüscher, C., and Slesinger, P. A. (2010) *Nat. Rev. Neurosci.* **11,** 301–315
15. Logothetis, D. E., Lupyan, D., and Rosenhouse-Dantsker, A. (2007) *J. Physiol.* **582,** 953–965
16. Nishida, M., Cadene, M., Chait, B. T., and MacKinnon, R. (2007) *EMBO J.* **26,** 4005–4015
17. Tao, X., Avalos, J. L., Chen, J., and MacKinnon, R. (2009) *Science* **326,** 1668–1674
18. Clarke, O. B., Caputo, A. T., Hill, A. P., Vandenberg, J. I., Smith, B. J., and Gulbis, J. M. (2010) *Cell* **141,** 1018–1029
19. Hansen, S. B., Tao, X., and Mackinnon, R. (2011) *Nature*
20. Proks, P., Antcliff, J. F., and Ashcroft, F. M. (2003) *EMBO Rep.* **4,** 70–75
21. Xiao, J., Zhen, X. G., and Yang, J. (2003) *Nat. Neurosci.* **6,** 811–818
22. Jarosławski, S., Zadek, B., Ashcroft, F., Vénien-Bryan, C., and Scheuring, S. (2007) *J. Mol. Biol.* **374,** 500–505
23. Kuo, A., Domene, C., Johnson, L. N., Doyle, D. A., and Vénien-Bryan, C. (2005) *Structure* **13,** 1463–1472
24. Inanobe, A., Matsuura, T., Nakagawa, A., and Kurachi, Y. (2007) *Channels* **1,** 39–45
25. Inanobe, A., Nakagawa, A., Matsuura, T., and Kurachi, Y. (2010) *J. Biol. Chem.* **285,** 38517–38523
26. Otwinowski, Z., and Minor, W. (1997) *Methods Enzymol.* **276,** 307–326
27. Collaborative Computational Project, Number Four (1994) *Acta Crystallogr. D. Biol. Crystallogr.* **50**, 760–763
28. Emsley, P., and Cowtan, K. (2004) *Acta Crystallogr. D. Biol. Crystallogr.* **60,** 2126–2132
29. Inanobe, A., Horio, Y., Fujita, A., Tanemoto, M., Hibino, H., Inageda, K., and Kurachi, Y. (1999) *J. Physiol.* **521,** 19–30
30. Inanobe, A., Matsuura, T., Nakagawa, A., and Kurachi, Y. (2011) *Biochem. Biophys. Res. Commun.* **407,** 366–371
31. Xu, Y., Shin, H. G., Szép, S., and Lu, Z. (2009) *Nat. Struct. Mol. Biol.* **16,** 1252–1258
32. Jiang, Y., and MacKinnon, R. (2000) *J. Gen Physiol.* **115,** 269–272
33. Lopatin, A. N., Makhina, E. N., and Nichols, C. G. (1994) *Nature* **372,** 366–369
34. Zeidner, G., Sadja, R., and Reuveny, E. (2001) *J. Biol. Chem.* **276,** 35564–35570
35. Guo, Y., Waldron, G. J., and Murrell-Lagnado, R. (2002) *J. Biol. Chem.* **277,** 48289–48294
36. Hilgemann, D. W., and Ball, R. (1996) *Science* **273,** 956–959
37. Huang, C. L., Feng, S., and Hilgemann, D. W. (1998) *Nature* **391,** 803–806
38. Zhang, H., He, C., Yan, X., Mirshahi, T., and Logothetis, D. E. (1999) *Nat. Cell Biol.* **1,** 183–188
39. Ito, H., Sugimoto, T., Kobayashi, I., Takahashi, K., Katada, T., Ui, M., and Kurachi, Y. (1991) *J. Gen Physiol.* **98,** 517–533
40. Nemec, J., Wickman, K., and Clapham, D. E. (1999) *Biophys. J.* **76,** 246–252
41. Pegan, S., Arrabit, C., Zhou, W., Kwiatkowski, W., Collins, A., Slesinger, P. A., and Choe, S. (2005) *Nat. Neurosci.* **8,** 279–287
42. Robertson, J. L., Palmer, L. G., and Roux, B. (2008) *J. Gen Physiol.* **132,** 613–632
43. Yang, J., Jan, Y. N., and Jan, L. Y. (1995) *Neuron* **14,** 1047–1054
44. Guo, D., and Lu, Z. (2003) *J. Gen Physiol.* **122,** 485–500

45. Xie, L. H., John, S. A., Ribalet, B., and Weiss, J. N. (2004) *J. Physiol.* **561,** 159–168
46. Fujiwara, Y., and Kubo, Y. (2006) *J. Gen Physiol.* **127,** 401–419
47. Matsuda, H., Saigusa, A., and Irisawa, H. (1987) *Nature* **325,** 156–159
48. Lu, Z. (2004) *Annu. Rev. Physiol.* **66,** 103–129
49. Yamashita, T., Horio, Y., Yamada, M., Takahashi, N., Kondo, C., and Kurachi, Y. (1996) *J. Physiol.* **493,** 143–156
50. Yan, D. H., and Ishihara, K. (2005) *J. Physiol.* **563,** 725–744
51. Pegan, S., Arrabit, C., Slesinger, P. A., and Choe, S. (2006) *Biochemistry* **45,** 8599–8606
52. Gupta, S., Bavro, V. N., D'Mello, R., Tucker, S. J., Vénien-Bryan, C., and Chance, M. R. (2010) *Structure* **18,** 839–846
53. DeLano, W. L. (2010) *The PyMOL Molecular Graphics System*, version 0.99rc6, Schrödinger, LLC, New York